IEEE Access
Multidisciplinary | Rapid Review | Open Access Journal

Received April 14, 2020, accepted May 24, 2020, date of publication June 2, 2020, date of current version June 17, 2020.

Digital Object Identifier 10.1109/ACCESS.2020.2999463

A Two-Step Method for Ionospheric Clutter Mitigation for HFSWR With Two-Dimensional Dual-Polarized Received Array

YUNLONG YANG, (Student Member, IEEE), XINGPENG MAO, (Member, IEEE), YUGUAN HOU, (Member, IEEE), AND JUN GENG, (Member, IEEE)

School of Electronics and Information Engineering, Harbin Institute of Technology, Harbin 150001, China
Key Laboratory of Marine Environmental Monitoring and Information Processing, Ministry of Industry and Information Technology, Harbin 150001, China

Corresponding author: Xingpeng Mao (mxp@ hit.edu.cn)

This work was supported by the Key Program of National Natural Science Foundation of China under Grant 61831009.

ABSTRACT For high-frequency surface wave radar (HFSWR), the unwanted radio wave originated from the ionosphere is commonly called ionospheric clutter. Its presence seriously affects the performance of the HFSWR and extremely degrades the radar capability to detect target over long distances. To solve this problem, this paper proposes a two-step method for ionospheric clutter mitigation with two-dimensional dual-polarized received array. The proposed method first performs parameter estimation of the clutter, and then gives a polarimetric-adaptive-based oblique projection filter (PAB-OPF) to suppress the clutter. In the first step, due to the fact that vertically and horizontally polarized antennas are at different array elements for reducing mutual coupling and hardware cost, 2-D DOAs are estimated to give phase compensation for polarization phase delay estimation. In the second step, the PAB-OPF is proposed to eliminate phase inconsistency by matching different polarization phase delays for different vertically polarized antennas, and then to suppress the clutter efficiently in space-polarization domain. Error analysis and computational complexity of the proposed method are derived. Experimental results are shown to illustrate the superiority of the proposed method for ionospheric clutter suppression.

INDEX TERMS High-frequency surface wave radar, dual-polarized array, ionospheric clutter, oblique projection, clutter mitigation.

I. INTRODUCTION

High-frequency surface wave radar (HFSWR) is capable of receiving surface vessel and low-flying aircraft echoes over much longer ranges than microwave radar. This is achieved by the long-distance propagation of the vertically polarized (V-POL) electromagnetic (EM) surface wave over the ocean surface, which can be regarded as the conductor. To minimize attenuation of surface wave, the HFSWR usually operates at the lower high frequency band (3-6 MHz) [1], [2]. In practice, however, some radio wave energy radiates vertically or obliquely and will be reflected by the earth's ionosphere in this band. These unwanted echoes originated from ionosphere are commonly called ionospheric clutter [3]–[7]. Generally, in the range-Doppler domain data for HFSWR, the ionospheric clutter with range extension can be separated roughly in range domain. It is noted that for Doppler domain in the same range, there are two major characteristics of ionospheric clutter, i.e., mean Doppler shift and Doppler spread, both of which have significant adverse effects on target detection [3]. Thus, the ionospheric clutter has been considered as the greatest limitation for HFSWR to achieve consistently good performance in long-distance detection.

Previous work has suggested that the ionospheric clutter exhibits some directional characteristics, which are different from those of the target echoes from ocean surface [3], [8]. Both azimuth and pitch angles of the ionospheric clutter and target may be different. Particularly, the pitch angle of the target is near to 90°, whereas that of the ionospheric clutter is significantly smaller than 90°. Therefore, two-dimensional (2-D) received arrays have been employed for HFSWR systems to sufficiently exploit the difference in both azimuth

The associate editor coordinating the review of this manuscript and approving it for publication was Fan Zhang.

and pitch angles between them, for better suppression performance [9]–[11]. To further improve the performance of clutter suppression, some mitigation methods have been investigated by using multi-domain, e.g., time-frequency domain [12], [13] and space-time domain [14], [15]. However, those methods are based on 1-D received array.

On the other hand, previous researches show that the dominant component of surface target echo in received data is V-POL wave, since its horizontally polarized (H-POL) wave is mostly absorbed by ocean surface. By comparison, the ionospheric clutter from sky usually appears as elliptically polarized wave in received data, indicating that the ionospheric clutter consists of V-POL and H-POL components [3], [16]. Hence, in polarization domain, the polarization angle of the target echo is close to 90°, while that of the ionospheric clutter is much smaller than 90°. To the best of our knowledge, by using the evident difference in polarization angle, several techniques for ionospheric clutter suppression have been explored based on polarization sensitive array [16]–[18]. However, the performance of these methods are still limited due to inaccurate estimation and inappropriate usage of the polarization phase delay, which are listed as follows:

(1) For reducing the mutual coupling and the hardware cost, V-POL and H-POL antennas are usually located at different array element positions in practice, which may lead to inaccurate estimation of the polarization phase delay. Specifically, the inter-antenna spacing between V-POL and H-POL antennas can introduce extra spatial phase information for polarized steering vector of the EM signal, which will have an adverse effect on estimation of polarization phase delay. This observation is hard to be noticed and hence the incorrect estimation of polarization phase delay contains such spatial phase information [17], [18]. And then, the filter constructed with such estimated polarization phase delay will suffer performance degradation.

(2) As the gain of the V-POL antenna at or near the vertical is very low, it is reasonable to suppose that the phase of the individual antennas in the vicinity of vertical direction are susceptible to manufacturing tolerance and, hence, there is a random variation among similar antennas [3]. This will lead to phase error among V-POL antennas in the vertical direction, resulting in phase inconsistency. In reality, the phase inconsistency among V-POL antennas can be reflected in different polarization phase delays for different V-POL antennas. Nevertheless, such phase inconsistency is usually ignored in the open literatures related with clutter mitigation [17], [18]. In this case, the performance of the existing methods may degrade.

In order to take advantages of multi-domain information (i.e., the space domain and polarization domain) for better clutter suppression and solve the above problems, this paper proposes a two-step mitigation method for HFSWR with a 2-D dual-polarized received array. In the first step of the proposed method, DOA and polarization state of the ionospheric clutter are estimated. Particularly, by using the estimated DOA, such introduced spatial phase information will be compensated in the estimation of polarization phase delay based on spatially separated EM vector sensor (SS-EMVS), in which the V-POL and H-POL antennas are located at different elements. Then, an polarimetric-adaptive-based oblique projection (OP) filter (PAB-OPF) based on space-polarization domain is constructed in the second step, to remove the effect of the phase inconsistency by matching different polarization phase delay and hence mitigate the ionospheric clutter efficiently.

The rest of this paper is organized as follows. Section II reviews the polarized signal model, HFSWR system with 2-D dual-polarized array and OP operator. Section III proposes the two-step method for ionospheric clutter mitigation. In section IV, the error analysis and computational complexity of the proposed method are given. Section V provides numerical examples to show the effectiveness of the proposed method. Finally, Section VI concludes this paper.

In this paper, scalars are denoted by lowercase italic letters, e.g., a. Vectors are denoted by italic boldface lowercase letters, e.g., $\boldsymbol{a}$. Matrices are denoted by italic boldface capital letters, e.g., $\boldsymbol{A}$. We list some notational conventions which will be used in the paper.

- $|a|$: absolute value of a
- $[\boldsymbol{a}]_i$: the ith item of a vector $\boldsymbol{a}$
- $||\boldsymbol{a}||_2$: the Euclidean norm for the vector $\boldsymbol{a}$
- $\boldsymbol{A}^*$: complex conjugate of $\boldsymbol{A}$
- $\boldsymbol{A}^{\mathrm{T}}$: transpose of $\boldsymbol{A}$
- $\boldsymbol{A}^{\mathrm{H}}$: conjugate transpose of $\boldsymbol{A}$
- angle($\boldsymbol{A}$): function to obtain the complex phase of $\boldsymbol{A}$
- E $\{\boldsymbol{A}\}$: mathematical expectation of $\boldsymbol{A}$
- $\boldsymbol{A} \odot \boldsymbol{B}$: Hadamard product of $\boldsymbol{A}$ and $\boldsymbol{B}$
- $\boldsymbol{I}_N$: an $N \times N$ identity matrix

II. PRELIMINARIES

In this section, we will first give a polarized signal model, review HFSWR system with 2-D dual-polarized array, and then briefly introduce the OP operator.

A. POLARIZED SIGNAL MODEL

We consider that one far-field narrowband, plane EM wave impinges on a collocated EMVS (C-EMVS). The C-EMVS is composed of two identical, but orthogonally oriented antennas, which are spatially collocated in a point-like geometry. In a Cartesian coordinate system, a C-EMVS located at origin point is shown in Fig. 1. Here, the two antennas paralleling to x-axis and z-axis are called H-POL antenna and V-POL antenna, respectively. $\theta \in [0, 90°]$ and $\phi \in [0, 360°)$ are the pitch angle measured from the positive z-axis and the azimuth angle measured from the positive x-axis, respectively. Since signal's polarization parameters (polarization angle and polarization phase delay) are usually described in a right-hand spherical coordinate system, a completely

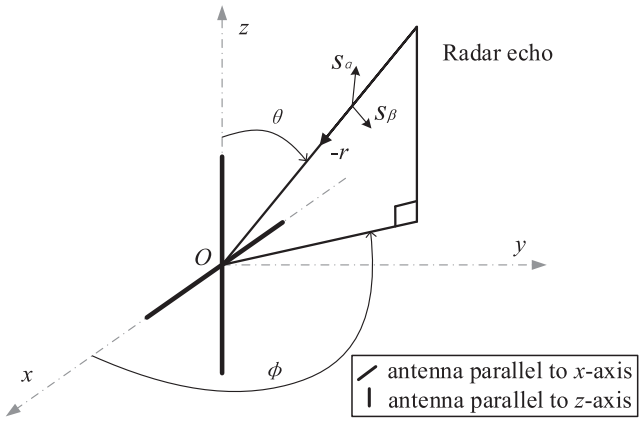

FIGURE 1. A C-EMVS composed of two identical, but orthogonally oriented antennas.

polarized wave received from a C-EMVS is given as [19]

$$\boldsymbol{J}(t)=\begin{bmatrix}J_z(t)\\J_x(t)\end{bmatrix}=\underbrace{\begin{bmatrix}-\sin\theta & 0\\ \cos\theta\cos\phi & -\sin\phi\end{bmatrix}\overbrace{\begin{bmatrix}\sin\varepsilon e^{j\eta}\\ \cos\varepsilon\end{bmatrix}}^{\boldsymbol{a}_p(\varepsilon,\eta)}}_{\bar{\boldsymbol{a}}_p(\theta,\phi,\varepsilon,\eta)}s(t), \quad (1)$$

where $s(t)$ denotes the signal's complex amplitude, and J_z and J_x represent a pair of orthogonal components in the Cartesian coordinate system. Here, $\bar{\boldsymbol{a}}_p(\theta,\phi,\varepsilon,\eta)$ and $\boldsymbol{a}_p(\varepsilon,\eta)$ are the signal's polarized steering vectors in the Cartesian coordinate system and right-hand spherical coordinate system, respectively. $\varepsilon\in[0,90°]$ and $\eta\in[0,360°]$ denote the polarization angle and polarization phase delay in the right-hand spherical coordinate system.

For the purpose of theoretical analysis and measured data processing, the expression form of $\bar{\boldsymbol{a}}_p(\theta,\phi,\varepsilon,\eta)$ can be rewritten as similar as the expression form of $\boldsymbol{a}_p(\varepsilon,\eta)$. Hence, we have

$$\boldsymbol{J}(t)=\underbrace{\begin{bmatrix}\sin\bar{\varepsilon}e^{j\bar{\eta}}\\ \cos\bar{\varepsilon}\end{bmatrix}}_{\bar{\boldsymbol{a}}_p(\bar{\varepsilon},\bar{\eta})}s(t), \quad (2)$$

where

$$\bar{\varepsilon}=\arctan\frac{|J_z|}{|J_x|},\quad \bar{\eta}=\text{angle}(J_z)-\text{angle}(J_x). \quad (3)$$

Here, $\bar{\varepsilon}\in[0,90°]$ and $\bar{\eta}\in[0,360°]$ denote the polarization angle and polarization phase delay in the Cartesian coordinate system, respectively.

B. HFSWR SYSTEM WITH 2-D DUAL-POLARIZED ARRAY

The monostatic radar which collected the data set presented in this paper is a HFSWR system located at Weihai city of Shandong province, China. This radar is capable of transmitting V-POL wave with frequency modulated interrupting continuous wave. The received array is a L-shaped polarization sensitive array composed of two orthogonal linear subarrays with 13 antennas, as shown in Fig. 2.

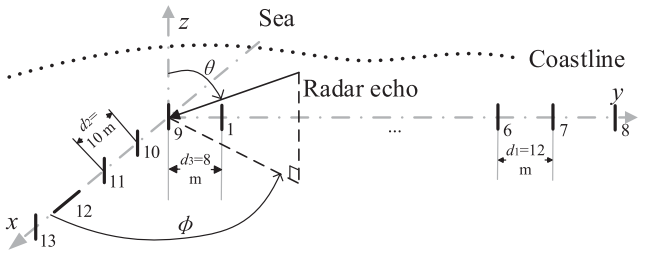

FIGURE 2. The L-shaped dual-polarized received array.

TABLE 1. Basic parameters of ionospheric clutters in RDP.

n	Range cell	Doppler cell
1	160 ~164	90 ~125
2	171 ~173	50 ~76 & 88 ~119

In Fig. 2, the uniform linear array (ULA) along y-axis, named as y-subarray, has 8 V-POL antennas, and the other array along x-axis, named as x-subarray, is composed of a H-POL antenna and a nonuniform linear array with 4 V-POL antennas. The antenna locations in y-subarray are at $\boldsymbol{L}_y=\begin{bmatrix}1&2&3&4&5&6&7&8\end{bmatrix}$. In the x-subarray, the V-POL antenna locations are at $\boldsymbol{L}_x=\begin{bmatrix}9&10&11&13\end{bmatrix}$, whereas the H-POL antenna is at the 12th element. The orientation of the H-POL antenna is parallel to x-axis.

To observe range and velocity characteristics of objects from radar echo, range-Doppler map (RDP) for experimental data sets is usually utilized. The RDP, which expresses range and Doppler power spectrum of a single channel at a time, uses 3-D mode to display. The range-Doppler domain data at a time is one single-snapshot data. So the data in the same range-Doppler cells of all channels can be considered as the array measurement with single-snapshot. In RDP, x-axis denotes Doppler information (also called velocity information), y-axis denotes range information, and z-axis expressed as color value denotes power spectrum.

A typical RDP demonstrating the data received from V-POL channel in aforesaid HFSWR is shown in Fig. 3. In this figure, the ionospheric clutters with a range extent of several range cells may come from the same direction [3]. Since these ionospheric clutters occur at ranges over 160 km, they become the main impediment on long-range direction. There are two pieces of ionospheric clutters in Fig. 3, and their basic parameters in RDP are listed in Table 1. A target is present at range-Doppler cell (49, 101) and its normalized power is −31.28 dB.

C. OBLIQUE PROJECTION OPERATOR

Consider matrices $\boldsymbol{A}\in\mathbb{C}^{n\times m_1}$ and $\boldsymbol{B}\in\mathbb{C}^{n\times m_2}$ are of full column ranks, and they are linearly independent from each other. Then we have $n\geq(m_1+m_2)$. Note that $\boldsymbol{A}$ is not required to be orthogonal to $\boldsymbol{B}$. Their subspaces are given as *span* $\{\boldsymbol{A}\}$ and *span* $\{\boldsymbol{B}\}$, respectively. An OP operator $\boldsymbol{E_{AB}}$ onto *span* $\{\boldsymbol{A}\}$ along *span* $\{\boldsymbol{B}\}$ can be defined as [20]

$$\boldsymbol{E_{AB}}=\boldsymbol{A}\left(\boldsymbol{A}^{\mathrm{H}}\boldsymbol{\Pi}_{\boldsymbol{B}}^{\perp}\boldsymbol{A}\right)^{-1}\boldsymbol{A}^{\mathrm{H}}\boldsymbol{\Pi}_{\boldsymbol{B}}^{\perp}, \quad (4)$$

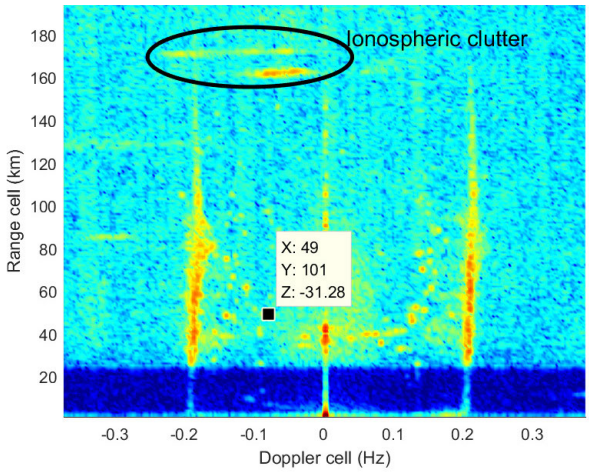

FIGURE 3. Range-Doppler map with ionospheric clutters.

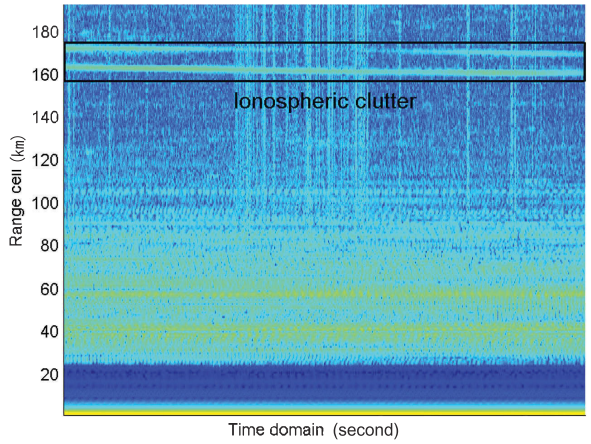

FIGURE 4. Range-time map with ionospheric clutter.

where $\boldsymbol{\Pi}_{\boldsymbol{B}}^{\perp} = \boldsymbol{I} - \boldsymbol{B}\left(\boldsymbol{B}^{\mathrm{H}}\boldsymbol{B}\right)^{-1}\boldsymbol{B}^{\mathrm{H}}$ is the orthogonal complement of $\boldsymbol{B}$. Then, we have [20]

$$\boldsymbol{E}_{\boldsymbol{AB}}\boldsymbol{A} = \boldsymbol{A}, \quad \boldsymbol{E}_{\boldsymbol{AB}}\boldsymbol{B} = \boldsymbol{0}. \tag{5}$$

It can be seen from (5) that the range of $\boldsymbol{E}_{\boldsymbol{AB}}$ is the subspace *span* $\{\boldsymbol{A}\}$ and the null space of $\boldsymbol{E}_{\boldsymbol{AB}}$ contains the subspace *span* $\{\boldsymbol{B}\}$.

III. TWO-STEP MITIGATION METHOD

A. 2-D DOA ESTIMATION

The range-time map (RTP) corresponding to RDP in Fig. 3 is also a 3-D surface plot, as shown in Fig. 4. For RTP, its x-axis, y-axis and z-axis represent range domain, time domain and intensity, respectively. In the first step of the proposed method, the 2-D DOA (θ_c, ϕ_c) of ionospheric clutter will be estimated from range-time domain data by using MUSIC algorithm [21]. The received signal $\boldsymbol{y}(t)$ for the range-time domain data in a single range cell can be expressed as

$$\boldsymbol{y}(t) = \boldsymbol{a}_s s(t) + \boldsymbol{a}_c c(t) + \boldsymbol{u}(t) + \boldsymbol{n}(t), \tag{6}$$

where $s(t)$, $c(t)$, $\boldsymbol{u}(t)$ and $\boldsymbol{n}(t)$ respectively denote the target signal, ionospheric clutter, sea clutter and the white Gaussian noise. $\boldsymbol{a}_s$ and $\boldsymbol{a}_c$ are the steering vectors of the potential target and ionospheric clutter, respectively. Compared with power of ionospheric clutter existing in the long distance (e.g., over 160 km in Fig. 3), the power of target and sea clutter in this distance are weak in range-time domain. Hence they do not affect the 2-D DOA estimation of ionospheric clutter. In this case, the received signal $\boldsymbol{y}(t)$ can be approximately rewritten as

$$\boldsymbol{y}(t) = \boldsymbol{a}_c c(t) + \boldsymbol{n}(t), \tag{7}$$

where

$$\begin{aligned} \boldsymbol{a}_c &= [\boldsymbol{a}_{c,y}\, \boldsymbol{a}_{c,x}]^{\mathrm{T}}, \\ \boldsymbol{a}_{c,y} &= [q\ qe^{-j[\Phi_y]_2}\ \cdots\ qe^{-j[\Phi_y]_8}], \\ \boldsymbol{a}_{c,x} &= [1\ e^{-j[\Phi_x]_2}\ \cdots\ e^{-j[\Phi_x]_4}], \end{aligned} \tag{8}$$

Here, $\boldsymbol{a}_{c,y}$ and $\boldsymbol{a}_{c,x}$ respectively are the spatial steering vectors of the ionospheric clutter based on y- and x-axes, and

$$\begin{aligned} q &= e^{-j\frac{2\pi d_3}{\lambda}\sin\theta_c \sin\phi_c}, \\ [\boldsymbol{\Phi}_y]_i &= \frac{2\pi d_1}{\lambda}\sin\theta_c \sin\phi_c([\boldsymbol{L}_y]_i - 1), \quad 1 \le i \le 8, \\ [\boldsymbol{\Phi}_x]_k &= \frac{2\pi d_2}{\lambda}\sin\theta_c \cos\phi_c([\boldsymbol{L}_x]_k - 9), \quad 1 \le k \le 4. \end{aligned} \tag{9}$$

Note that the 9th array element (see Fig. 2) is considered as the reference element for steering vectors in (8). Hence q is the spatial phase delay information introduced by the spacing d_3 between x- and y-subarrays. $d_1 = 12$ m, $d_2 = 10$ m and $d_3 = 8$ m, as shown in Fig. 2. $[\boldsymbol{L}_y]_k$ and $[\boldsymbol{L}_x]_k$ denote the element positions from the kth item in $\boldsymbol{L}_y$ and $\boldsymbol{L}_x$, respectively. The autocorrelation matrix of the received signal in (7) is given as

$$\boldsymbol{R} = \mathrm{E}\left\{\boldsymbol{y}(t)\boldsymbol{y}(t)^{\mathrm{H}}\right\} = \boldsymbol{a}_c\sigma_c^2\boldsymbol{a}_c^{\mathrm{H}} + \sigma_n^2\boldsymbol{I}_{12}, \tag{10}$$

where σ_c^2 and σ_n^2 denote the power of the ionospheric clutter and noise, respectively. Hence the MUSIC algorithm can be applied for (10).

The DOA estimation of the ionospheric clutter is listed in Table 2. Note that the DOA estimation of the ionospheric clutter is averaged over several continuous range cells.

TABLE 2. DOA estimation of ionospheric clutter.

	pitch angle	azimuth angle
clutter in range cells (160 ~164)	14°	123.4°
clutter in range cells (171 ~173)	8.6°	217.3°

B. POLARIZATION STATE ESTIMATION IN RANGE-DOPPLER DOMAIN

The polarization state (i.e., polarization angle and polarization phase delay) of the ionospheric clutter will be estimated in range-Doppler domain. After amplitude normalization for suppressing the amplitude inconsistency, the polarization angle $\varepsilon_c(l, r)$ of the range-Doppler cells (l, r) masked by the ionospheric clutter is given as

$$\varepsilon_{c,m}(l, r) = \arctan\left(\frac{|V_m(l, r)|}{|H(l, r)|}\right), \tag{11}$$

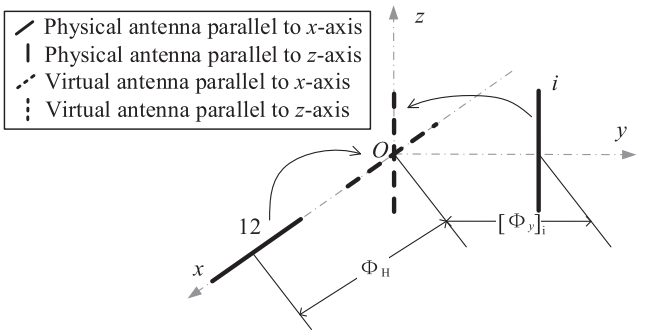

FIGURE 5. A SS-EMVS and its virtual dual-polarized C-EMVS at origin point.

where $H(l, r)$ and $V_m(l, r)$ denote the samples of the H-POL channel and the mth V-POL channel (which corresponds to the $[a_c]_m$) at the range-Doppler cell (l, r), respectively. And then, similar to (3) based on C-EVMS, the polarization phase delay $\eta_{c,m}(l, r)$ is directly from measured data [17], [18], i.e.,

$$\eta_{c,m}(l, r) = \text{angle}(V_m(l, r)) - \text{angle}(H(l, r)). \tag{12}$$

It is noted that, for reducing the mutual coupling between the V-POL and H-POL antennas and saving the hardware cost in practice, the V-POL and H-POL antennas are located at different elements in the received array [17], [18] and in Fig. 2. In this case, the pair of the H-POL antenna and any one V-POL antenna can be regarded as a SS-EMVS composed of two spatially separated antennas. For example, the SS-EMVS which consists of the H-POL antenna (at the 12th element in x-subarray) and the V-POL antenna (at the ith element in y-subarray) is shown in Fig. 5. Here, considering origin point as reference point, $\Phi_H = \frac{6\pi d_2}{\lambda} \sin\theta_c \cos\phi_c$ and $[\boldsymbol{\Phi}_y]_i$ denote the spatial phase delays of the physical H-POL and V-POL antennas, respectively. One can see that in Fig. 5, the spacing between the V-POL and H-POL antennas exists, and then the extra spatial phase information Φ_H and $[\boldsymbol{\Phi}_y]_i$ are introduced in polarized steering vector. Hence, $\eta_{c,m}(l, r)$ estimated from (12) contains such spatial phase information and is incorrect for received array in references [17], [18] and Fig. 2.

In order to solve the problem, we will construct a virtual dual-polarized C-EMVS at origin point for the corresponding SS-EMVS to obtain the accuracy estimation of polarization phase delay, as shown in Fig. 5. Specifically, the introduced spatial phase information will be eliminated by using the transformable relationship on spatial phase delay between co-polarization antennas in SS-EMVS and virtual C-EMVS. To this end, the polarized steering vector based on the SS-EMVS is given as

$$\boldsymbol{a}_p(\varepsilon_{c,m}(l, r), \dot{\eta}_{c,m}(l, r)) = \begin{bmatrix} \sin\varepsilon_{c,m}(l, r) e^{j\dot{\eta}_{c,m}(l,r)} \\ \cos\varepsilon_{c,m}(l, r) \end{bmatrix}, \tag{13}$$

where $\dot{\eta}_{c,m}(l, r)$ is the polarization phase delay of ionospheric clutter based on SS-EMVS, and the polarized steering vector based on the corresponding C-EMVS is given as

$$\boldsymbol{a}_p(\varepsilon_{c,m}(l, r), \ddot{\eta}_{c,m}(l, r)) = \begin{bmatrix} \sin\varepsilon_{c,m}(l, r) e^{j\ddot{\eta}_{c,m}(l,r)} \\ \cos\varepsilon_{c,m}(l, r). \end{bmatrix} \tag{14}$$

where $\ddot{\eta}_{c,m}(l, r)$ denotes the polarization phase delay of ionospheric clutter based on virtual C-EMVS. Depending on spatial phase delay, the relationship on polarization phase delays between SS-EMVS and C-EMVS is

$$\dot{\eta}_{c,m}(l, r) = \ddot{\eta}_{c,m}(l, r) + j\ln[a_c]_m - \Phi_H \tag{15}$$

Thus, recalling (3), we have

$$\begin{aligned} \ddot{\eta}_{c,m}(l, r) = {} & \text{angle}(V_m(l, r)) + \Phi_H \\ & - (\text{angle}(H(l, r)) + j\ln[a_c]_m), \end{aligned} \tag{16}$$

where

$$\begin{aligned} j\ln[\boldsymbol{a}_c]_m &= [\boldsymbol{\Phi}_y]_m, \quad 1 \le m \le 8, \\ j\ln[\boldsymbol{a}_c]_m &= [\boldsymbol{\Phi}_x]_{m-8}, \quad 9 \le m \le 12. \end{aligned} \tag{17}$$

In (16), $j\ln[\boldsymbol{a}_c]_m$ and Φ_H respectively can be considered as the phase compensations for the mth V-POL antenna and the H-POL antenna in SS-EMVS, to give precise estimation of polarization phase delay. Comparing polarization phase delay estimated from (12) with (16), one can see that $\eta_{c,m}(l, r)$ estimated in previous work contains extra phase information of antenna locations. In this case, such phase information will be repeatedly calculated in space-polarization domain based filter, resulting in performance degradation of clutter suppression.

C. POLARIMETRIC-ADAPTIVE-BASED OBLIQUE PROJECTION FILTER (PAB-OPF) IN RANGE-DOPPLER DOMAIN

In RDP, the power of ionospheric clutter and target signal is limited in concentrated on limited range-Doppler cells, which significantly increases the clutter-to-noise ratio and signal-to-noise ratio. Then the filtering process of clutter mitigation is based on the range-Doppler domain data. Due to the similarity of adjacent range-Doppler in each range cell [22], the estimation of polarization angle and polarization phase delay are averaged for each range cell to give the polarization state estimation of the ionospheric clutter. For example, the estimations of polarization angle ε_c and polarization phase delay η_c (from (16)) of ionospheric clutter in the 162th range cell is provided in Table 3. In this table, one can see that the estimations of polarization angles are essentially the same for all V-POL antennas due to amplitude normalization. Thus ε_c can be obtained by averaging all $\varepsilon_{c,m}$ and then used for filter construction in practice. Note that the estimations of polarization phase delays are significantly different from each other, which shows the phase inconsistency among V-POL antennas.

Considering (7), the signal model in the range-Doppler domain is expressed as

$$\begin{aligned} \boldsymbol{y}(l, r) &= \begin{bmatrix} V_1(l, r) & \cdots & V_{12}(l, r) & H(l, r) \end{bmatrix}^{\mathrm{T}} \\ &= \boldsymbol{a}_{sp,t} s(l, r) + \boldsymbol{a}_{sp,c} c(l, r) + \boldsymbol{n}(l, r), \end{aligned} \tag{18}$$

TABLE 3. Polarization state estimation of ionospheric clutter.

	1	2	3	4	5	6	7	8	9	10	11	13
polarization angle (°)	55.7	55.4	55.5	55.8	56.9	57.3	57.1	57.2	56.6	57.8	57.7	57.5
polarization phase delay (°)	323.6	106.1	122.5	137.0	298.2	195.9	180.8	213.0	86.3	105.9	129.8	165.1

where $s(l, r)$, $c(l, r)$ and $\boldsymbol{n}(l, r)$ denote potential target, clutter and noise at range-Doppler cell (l, r), respectively. $\boldsymbol{a}_{sp,t}$ and $\boldsymbol{a}_{sp,c}$ are the space-polarization-domain steering vectors of the target signal and ionospheric clutter, respectively.

In previous work [23]–[25], $\boldsymbol{a}_{sp,c}$ is usually modeled as

$$\boldsymbol{a}_{sp,c} = \begin{bmatrix} \boldsymbol{a}_c \\ e^{-jD_2 \sin\theta_c \cos\phi_c \cdot 3} \end{bmatrix} \odot \begin{bmatrix} \sin\varepsilon_c e^{j\eta_c} \\ \vdots \\ \sin\varepsilon_c e^{j\eta_c} \\ \cos\varepsilon_c \end{bmatrix}. \tag{19}$$

Here, it can be seen that, whatever η_c is estimated from (12) or (16), η_c is set to be same for all items in (19) which correspond to all V-POL antennas. In practice, however, η_c estimated from different V-POL antennas are different in measured data, due to phase inconsistency (see Table 3). Thus the mismatch between data model and measured data will lead to performance degradation of clutter mitigation.

In order to reduce the adverse effect of the phase inconsistency, a PAB-OPF is proposed for ionospheric clutter mitigation. Depending on precisely estimated parameters in previous subsection, the space-polarization-domain steering vectors of the ionospheric clutter and the target are given as

$$\ddot{\boldsymbol{a}}_{sp,c} = \begin{bmatrix} \boldsymbol{a}_c \\ e^{-jD_2 \sin\theta_c \cos\phi_c \cdot 3} \end{bmatrix} \odot \begin{bmatrix} \sin\varepsilon_c e^{j\ddot{\eta}_{c,1}} \\ \vdots \\ \sin\varepsilon_c e^{j\ddot{\eta}_{c,9}} \\ \cos\varepsilon_c \end{bmatrix}, \tag{20}$$

and

$$\boldsymbol{a}_{sp,t} = \begin{bmatrix} \boldsymbol{a}_t \\ e^{-jD_2 \sin\theta_t \cos\phi_t \cdot 3} \end{bmatrix} \odot \begin{bmatrix} \sin\varepsilon_t e^{j\eta_t} \\ \vdots \\ \sin\varepsilon_t e^{j\eta_t} \\ \cos\varepsilon_t \end{bmatrix}, \tag{21}$$

where ε_t and η_t respectively denote the polarization angle and polarization phase delay of potential target, and $\boldsymbol{a}_t = [\boldsymbol{a}_{t,y}\ \boldsymbol{a}_{t,x}]^{\mathrm{T}}$ with $\boldsymbol{a}_{t,y} = [q\ \cdots\ qe^{-j\frac{2\pi d_1}{\lambda}\sin\theta_t \sin\phi_t([S_y]_8-1)}]^{\mathrm{T}}$ and $\boldsymbol{a}_{t,x} = [1\ \cdots\ e^{-j\frac{2\pi d_2}{\lambda}\sin\theta_t \cos\phi_t([S_x]_4-9)}]^{\mathrm{T}}$.

In (20), one can see that the polarization phase delay $\ddot{\eta}_{c,m}$ estimated from the mth V-POL antenna is located at the mth element of $a_{sp,c}$. This illustrates that $\ddot{\eta}_{c,m}$ in $a_{sp,c}$ is adaptive to the mth V-POL antenna for matching its polarization phase delay, resulting in removing the phase inconsistency efficiently.

Then the PAB-OPF is constructed as

$$\boldsymbol{w}_{sp} = (\boldsymbol{F}_0 \boldsymbol{E}_{t,c})^{\mathrm{H}}, \tag{22}$$

where $\boldsymbol{F}_0 = (\boldsymbol{a}_{sp,t}^{\mathrm{H}} \boldsymbol{a}_{sp,t})^{-1} \boldsymbol{a}_{sp,t}^{\mathrm{H}}$ and the OP operator is

$$\boldsymbol{E}_{t,c} = \boldsymbol{a}_{sp,t} (\boldsymbol{a}_{sp,t}^{\mathrm{H}} \Pi_{\ddot{\boldsymbol{a}}_{sp,c}}^{\perp} \boldsymbol{a}_{sp,t})^{-1} \boldsymbol{a}_{sp,t}^{\mathrm{H}} \Pi_{\ddot{\boldsymbol{a}}_{sp,c}}^{\perp}. \tag{23}$$

According to (5), the output of PAB-OPF at range-Doppler cell (l, r) is provided as

$$\begin{aligned} z(l, r) &= \boldsymbol{w}_{sp}^{\mathrm{H}} \boldsymbol{y}(l, r) \\ &= \boldsymbol{w}_{sp}^{\mathrm{H}} (\boldsymbol{a}_{sp,t} s(l, r) + \ddot{\boldsymbol{a}}_{sp,c} c(l, r) + \boldsymbol{n}(l, r)) \\ &= s(l, r) + \boldsymbol{w}_{sp}^{\mathrm{H}} \boldsymbol{n}(l, r). \end{aligned} \tag{24}$$

From (24), one can see that by using the PAB-OPF, the potential target signal is recovered with no distortion, whereas the ionospheric clutter is mitigated completely in the presence of antenna phase inconsistency.

IV. PERFORMANCE ANALYSIS

A. ERROR ANALYSIS

As mentioned above, the performance of the PAB-OPF depends mainly on two factors, i.e., precisely estimation of parameters and an exact matching between data model and measured data. Specifically, for η_c, either incorrect estimation or mismatch will lead to mitigation performance loss. As the proposed method is aimed to improve signal-to-clutter ratio (SCR), it is necessary to analyze the effects of those two factors on residual clutter in the output of the PAB-OPF.

Suppose $\hat{\eta}_c$ is the estimation of $\ddot{\eta}_{c,m}$ in previous work [17], [18], [23]–[25], and other parameters are estimated precisely. In the previous work, $\hat{\eta}_c$ contains space phase information of antenna location and is set to be same for all V-POL antennas. Then we have $\Delta\eta_{c,m} = \ddot{\eta}_{c,m} - \hat{\eta}_c$. Hence the weight steering vector of the PAB-OPF is expressed as

$$\boldsymbol{w}'_{sp} = (\boldsymbol{F}_0 \boldsymbol{E}'_{t,c})^{\mathrm{H}}, \tag{25}$$

where

$$\boldsymbol{E}'_{t,c} = \boldsymbol{a}_{sp,t} (\boldsymbol{a}_{sp,t}^{\mathrm{H}} \Pi_{\boldsymbol{a}'_{sp,c}}^{\perp} \boldsymbol{a}_{sp,t})^{-1} \boldsymbol{a}_{sp,t}^{\mathrm{H}} \Pi_{\boldsymbol{a}'_{sp,c}}^{\perp}. \tag{26}$$

Here, $\boldsymbol{a}'_{sp,c}$ is defined as (19) with replacing η_c by $\hat{\eta}_c$. Note that for any $\hat{\eta}_c$ for $\boldsymbol{a}'_{sp,c}$, when $\boldsymbol{a}_{sp,t}$ is precise, the target in the PAB-OPF output can be recovered without distortion due to the property of oblique projection (see (5)). Additionally, since the proposed method can not deal with noise, the error analysis focuses mainly on handling clutter (i.e., $c(l, r)$) with PAB-OPF. Then the residual clutter $z'(l, r)$ in the output of the PAB-OPF can be provided as

$$z'(l, r) = (\boldsymbol{w}'_{sp})^{\mathrm{H}} \ddot{\boldsymbol{a}}_{sp,c} c(l, r) = (\boldsymbol{w}'_{sp})^{\mathrm{H}} \Delta \boldsymbol{B} \boldsymbol{a}'_{sp,c} c(l, r)$$

$$= C\boldsymbol{a}_{sp,t}^{\mathrm{H}}\Pi_{\boldsymbol{a}'_{sp,c}}^{\perp}\underbrace{\begin{bmatrix} e^{j\Delta\eta_{c,1}} & 0 & 0 & 0 \\ 0 & \ddots & 0 & 0 \\ 0 & 0 & e^{j\Delta\eta_{c,12}} & 0 \\ 0 & 0 & 0 & 1 \end{bmatrix}}_{\Delta\boldsymbol{B}}\boldsymbol{a}'_{sp,c}c(l,r)$$

$$= C\boldsymbol{a}_{sp,t}^{\mathrm{H}}(\Delta\boldsymbol{B}\boldsymbol{a}'_{sp,c} - \frac{D}{B}\boldsymbol{a}'_{sp,c})c(l,r)$$

$$= C\boldsymbol{a}_{sp,t}^{\mathrm{H}}(\Delta\boldsymbol{B} - \frac{D}{B}\boldsymbol{I})\boldsymbol{a}'_{sp,c}c(l,r) \tag{27}$$

where

$$\begin{aligned} A &= \boldsymbol{a}_{sp,t}^{\mathrm{H}}\boldsymbol{a}_{sp,t} = M\cdot\sin^2\varepsilon_t + \cos^2\varepsilon_t, \\ B &= \boldsymbol{a}_{sp,c}^{\mathrm{H}}\boldsymbol{a}_{sp,c} = M\cdot\sin^2\varepsilon_c + \cos^2\varepsilon_c, \\ C &= A - ||\boldsymbol{a}_{sp,t}^{\mathrm{H}}\boldsymbol{a}_{sp,c}||_2^2, \\ D &= \sin^2\varepsilon_c\sum_{m=1}^{M}e^{j\Delta\eta_{c,m}} + \cos^2\varepsilon_c. \end{aligned} \tag{28}$$

Here, M is the number of V-POL antennas in the received array. Then, the power $P_c(l,r)$ of the residual clutter at range-Doppler cell (l,r) is $P_c(l,r) = \boldsymbol{z}'(l,r)(\boldsymbol{z}'(l,r))^{\mathrm{H}}$.

Theoretically, when $\ddot{\eta}_{c,m}$ is estimated precisely and the exact matching between data model and measured data is achieved, we have $\Delta\eta_{c,m} = 0$. In this condition, $(\Delta\boldsymbol{B} - \frac{D}{B}\boldsymbol{I}) = 0$, and then $\boldsymbol{z}'(l,r) = 0$, indicating that there is no residual clutter in the output. On the contrary, if $\Delta\eta_{c,m} \neq 0$, then $(\Delta\boldsymbol{B} - \frac{D}{B}\boldsymbol{I}) \neq 0$. In this case, $P_c(l,r) \neq 0$ and there exists residual clutter which decreases SCR and may mask the target signal.

B. COMPUTATIONAL COMPLEXITY

The computation of the proposed two-step method is provided in this subsection. Note that the first step is divided into two parts, i.e., DOA estimation and polarization state estimation, to give the computational complexity.

1) DOA ESTIMATION

For ionospheric clutter, the covariance matrix $\boldsymbol{R}$ is used for 2-D DOA estimation by using MUSIC algorithm, which takes about $O(M^3)$ operations for eigenvalue decomposition (EVD) and $O(\frac{90}{\Delta\alpha}\frac{360}{\Delta\beta}(M-1)(2M+1))$ for 2-D searching. Here, $\Delta\alpha$ and $\Delta\beta$ denote the searching intervals of the MUSIC in the pitch and azimuth angles, respectively. Hence, the complexity of this part is about $O(M^3 + \frac{90}{\Delta\alpha}\frac{360}{\Delta\beta}(M-1)(2M+1))$.

2) POLARIZATION STATE ESTIMATION

Assume the number of range-Doppler cells polluted by ionospheric clutter is K. Thus, the complexity of polarization angle estimated by (11) takes $O(K)$ operations, and the complexity of polarization phase delay estimated by (16) takes $O(6K)$ operations. Therefore the complexity of this part is about $O(7K)$.

3) PAB-OPF

The computational complexity of this step for each range-Doppler cell is dominated by the construction of OP operator. The cost for the OP operator is mainly caused by the construction and inverse of $(\boldsymbol{a}_{sp,t}^{\mathrm{H}}\Pi_{\boldsymbol{a}_{sp,c}}^{\perp}\boldsymbol{a}_{sp,t})$, which are about $O(M^2)$ and $O(M^3)$, respectively. Therefore the computational complexity of this step for K range-Doppler cells is about $O(KM^2 + KM^3)$.

Hence, the total computational complexity of the proposed two-step method is

$$O\left\{M^3 + \frac{90}{\Delta\alpha}\frac{360}{\Delta\beta}(M-1)(2M+1) + 7K + KM^2 + KM^3\right\}. \tag{29}$$

V. NUMERICAL RESULTS

In order to verify the efficiency of the proposed method, we will first give the numerical simulation and then use real HFSWR data to compare with the existing method.

A. NUMERICAL SIMULATION

The structure of received array for numerical simulation is the same with that in Fig. 2. the inter-spacing between antennas is set to be $d = \lambda/2$.

1) ESTIMATION OF POLARIZATION PHASE DELAY

This subsection first shows the estimations of polarization phase delay from different methods without phase inconsistency (as the first scenario), and then shows those in the case of phase inconsistency (as the second scenario). Assume that an EM signal at $(\theta,\varepsilon,\eta) = (70^\circ, 40^\circ, 30^\circ)$ impinges on this array. we will show the simulation on η estimation with varied azimuth angles ϕ from 135° to 225°, to verify the effectiveness of the proposed method. The simulation results with first three V-POL antennas are used for comparison.

The results of the first scenario are given in Fig. 6(a). In this figure, the estimations of η from (12) and (16) are shown. Specifically, η estimated by (16) equals to 30° for all three antennas, whereas η estimated by (12) varies differently with varied azimuth angles. This observation indicates that the proposed method can provide precise estimation for η, while the estimation of η from (12) is incorrect due to containing spatial phase information.

The results of the second scenario are given in Fig. 6(b). In this figure, the estimation of η also varies differently with varied azimuth angles, indicating that it is incorrect for (19). Furthermore, η estimated from different V-POL antennas by using (16) are different constants for all azimuth angles, which illustrates that the phase inconsistency among antennas has an effect on η estimation.

2) ERROR ANALYSIS

In this part, the parameters of target signal are set to be $(\phi_t,\theta_t,\varepsilon_t,\eta_t) = (175^\circ, 90^\circ, 88^\circ, 30^\circ)$, and the parameters of the clutter are the same with those in the previous part.

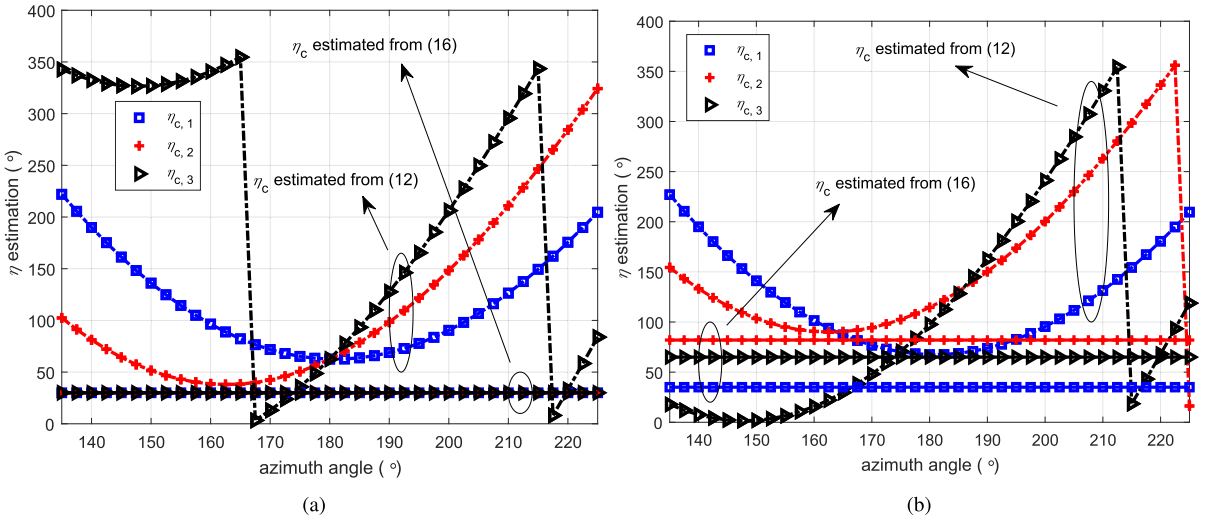

FIGURE 6. (a) η estimation without phase inconsistency. (b) η estimation in the case of phase inconsistency.

Both the power of target and clutter are set to be 1. Here, in the case of SNR $=$ 10 dB, the incorrect estimation of η_c and phase inconsistency for clutter suppression are shown in Fig. 7, respectively. From this figure, the power of residual clutter at output of PAB-OPF is close to zero and essentially constant for all azimuth angles, which illustrates that the proposed method can precisely estimate η and effectively reduce the phase inconsistency among V-POL antennas. As a contrast, in the case of incorrect estimation of η or existing phase inconsistency, the power of residual clutter at output of OPF is much greater than that at output of PAB-OPF and dramatically changes with the change of azimuth angles, indicating that both these two factors have adverse effects on clutter mitigation.

B. EXPERIMENTAL PERFORMANCE EVALUATION

In this subsection, we will verify the efficiency of the proposed method for ionospheric clutter mitigation. The multi-domain filtering algorithm [25] is used for comparison. The sensor array used in this subsection is given in Fig. 2, and the real HFSWR data introduced in Fig. 3 is used. Since we do not know whether there is a target existing in a range-Doppler cell polluted by clutter, the real target which located at range-Doppler cell (49, 101) is used to evaluate the effect of filtering on reserving the target. As the pitch angle θ_t of the target from ocean surface is very close to 90°, the azimuth angle of the target at cell (49, 101) is estimated by using digital beamforming. Specifically, the array output for cell (49, 101) can be regarded as the received data $\boldsymbol{y}(l, r, \phi_t) = \boldsymbol{a}_t(\phi_t)s(l, r) + \boldsymbol{n}(l, r)$, where the structure of $\boldsymbol{a}_t$ is the same with that of $\boldsymbol{a}_c$ in (8). Then the weight vector of digital beamforming can be provided as $\boldsymbol{y}(l, r, \phi_k)$ with $\phi_k (k = 1, \cdots, K)$ denoting the angle in the range of interest. The output of digital beamforming is $P_{\mathrm{DBF}}(k) = (\boldsymbol{y}(l, r, \phi_k))^{\mathrm{H}}\boldsymbol{y}(l, r, \phi_t)$. Then ϕ_k which corresponds to the maximum power of the output is the estimation of azimuth angle of target. By using digital beamforming, the azimuth of target signal at cell (49, 101) is estimated as 155.4°.

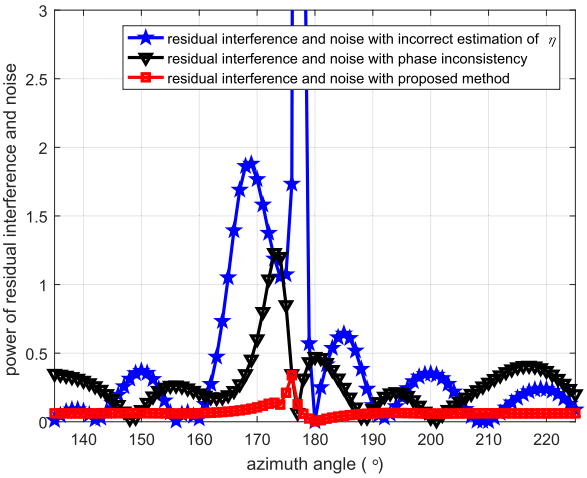

FIGURE 7. Power of residual clutter and noise under different η for OPF construction.

The range-Doppler map after ionospheric clutter mitigation by the multi-domain filtering algorithm and the proposed method is shown in Figs. 8 and 9, respectively. For target signal, its normalized power is −30.82 dB in Fig. 8 and is −31.25 dB in Fig. 9, which is substantially identical with the power of this target in original range-Doppler map. This illustrates that the target signal can be preserved effectively by both two methods. On the other hand, the ionospheric clutters are not be suppressed completely in Fig. 8, whereas they are mitigated significantly in Fig. 9. This observation indicates that the proposed method can provide precise estimation of polarization phase delay and eliminate phase inconsistency efficiently for clutter suppression.

Additionally, in each range cell of the range-Doppler domain data, the colors of range-Doppler cells with only

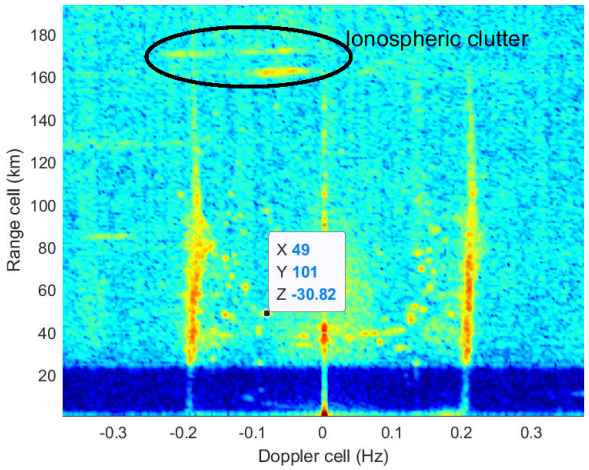

FIGURE 8. RDP after ionospheric clutter mitigation by the multi-domain filtering algorithm [25].

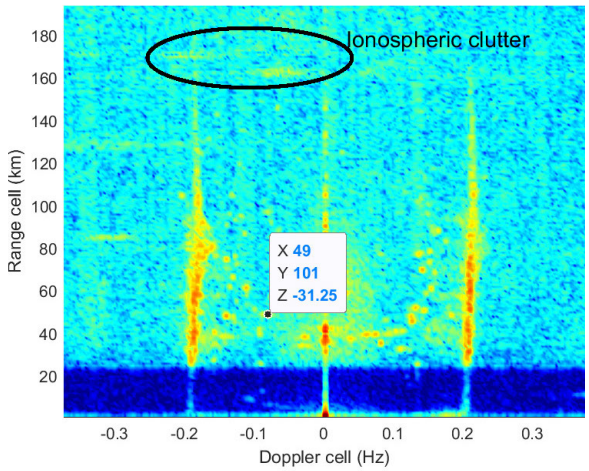

FIGURE 9. RDP after ionospheric clutter mitigation by the proposed method.

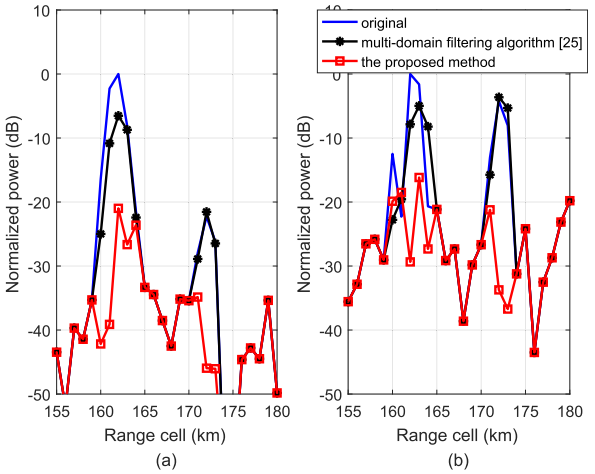

FIGURE 10. (a) Results of the multi-domain filtering algorithm and the proposed method at −0.070 Hz. (b) Results of the multi-domain filtering algorithm and the proposed method at −0.053 Hz.

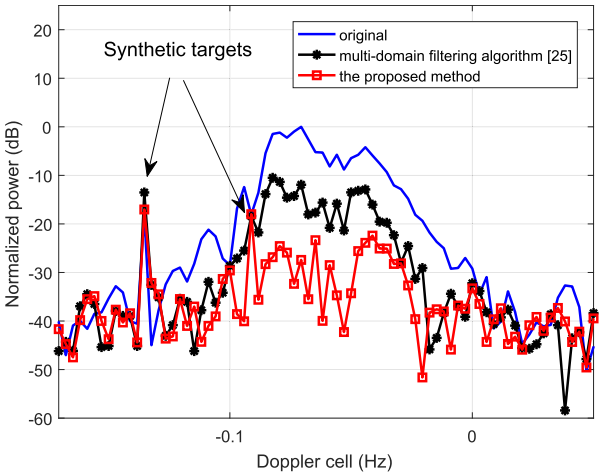

FIGURE 11. Results of the multi-domain filtering algorithm and the proposed method at range cell 162.

noise are essentially the same, which indicates that the noise powers are basically the same in the whole Doppler frequency domain in reality. Furthermore, when the range-Doppler cell occupied by clutter has no target, the output of the filter only contains noise power. In this case, the color denoting the output is essentially the same with that of range-Doppler cells with only noise. These observations show that the output in simulation results is basically in accordance with the theoretical assumption of the white Gaussian noise in (7).

Moreover, two slices at −0.070 Hz and −0.053 Hz from Figs. 3, 8 and 9 are chosen arbitrarily, and provided in Figs. 10(a) and 10(b), respectively. It can be seen from Fig. 10 that for each range-Doppler cell polluted by the clutter, the proposed method can provide significant clutter suppression performance (at least about 20 dB, almost surely), whereas strong ionospheric clutters exist in the output of the contrast method.

To further demonstrate the superiority of the proposed method, two synthetic targets, the parameters of which are the same with these of real target, are added in range cell 162. For the purposes of comparison, one synthetic target is added in range-Doppler cell (162, 82) which is not polluted by ionospheric clutter, and the other one is added in range-Doppler cell (162, 97) which is polluted by the ionospheric clutter. The results of the multi-domain filtering algorithm and the proposed method at range cell 162 are given in Fig. 11. In this figure, two synthetic targets are preserved by the multi-domain filtering algorithm and the proposed method. The power of ionospheric clutter is decreased by at least 20 dB and close to the power of background noise in the result of the proposed method, whereas the power attenuation of most part of the ionospheric clutter is much smaller than 20 dB in the result of the multi-domain filtering algorithm [25]. It is because that the incorrect estimation of η_c and phase mismatch between data model and measured data are present in the multi-domain filtering algorithm, leading to performance loss. Hence the performance of ionospheric clutter mitigation of the proposed method is better than that of the multi-domain filtering algorithm.

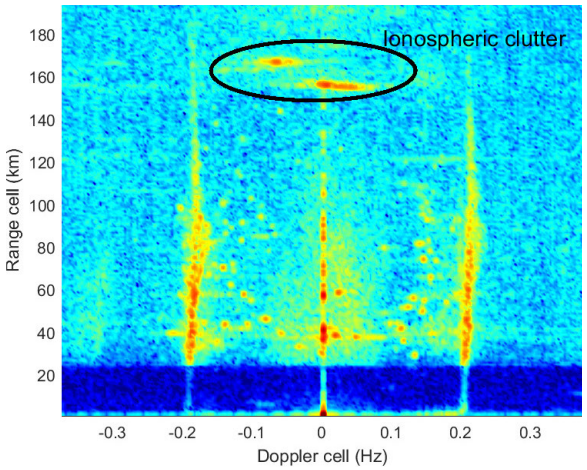

FIGURE 12. Range-Doppler map with ionospheric clutters.

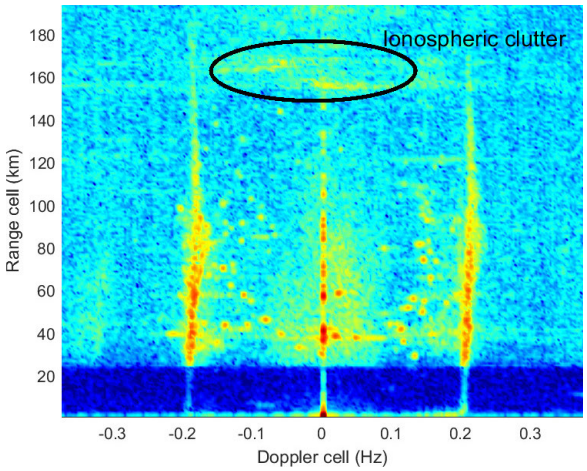

FIGURE 13. Result of the proposed method.

In order to verify the extensive applications of the proposed method, we use another real data received from the same array (i.e., Fig. 2) for demonstration. Such real HFSWR data with ionospheric clutter is given in Fig. 12. The result of the proposed method applied to this data for clutter suppression is shown in Fig. 13. It can be seen that the clutter has been largely suppressed in Fig. 13, indicating that the proposed method is valid in practice.

VI. CONCLUSION

We have proposed a two-step method for ionospheric clutter mitigation for HFSWR with a L-shaped dual-polarized received array. In the first step of the proposed method, DOA and polarization state of ionospheric clutter and target signal are estimated effectively. Particularly, the introduced spatial phase information in the estimation of polarized phase delay is compensated by estimated DOA. Then in the second step, the PAB-OPF is constructed with such precise estimation to reduce the effect of phase inconsistency and give good performance of clutter suppression. Theoretical analysis is provided to demonstrate the superior performance of the proposed method for ionospheric clutter mitigation. And experimental performance evaluation illustrates that the proposed method could achieve attenuation of clutter suppression at least 20 dB.

REFERENCES

[1] H. C. Chan, "Iceberg detection and tracking using high frequency surface wave radar," Defence Res. Establishment Ottawa, Ottawa, ON, Canada, Tech. Rep. 1310, 1997.
[2] H. C. Chan, "Detection and tracking of low-altitude aircraft using HF surface-wave radar," Defence Res. Establishment Ottawa, Ottawa, ON, Canada, Tech. Rep. 1334, 1998.
[3] H. C. Chan, *Characterization of Ionospheric Clutter in HF Surface-Wave Radar*. Ottawa, ON, Canada: Defence R&D, 2003.
[4] X. Yang, C. Yu, A. Liu, L. Wang, and T. Quan, "The vertical ionosphere parameters inversion for high frequency surface wave radar," *Int. J. Antennas Propag.*, vol. 2016, pp. 1–8, Dec. 2016.
[5] L. Zhe, Y. ChangJun, and L. AiJun, "Prediction method for ionospheric clutter suppression for HFSWR," *Electron. Lett.*, vol. 55, no. 15, pp. 857–859, Jul. 2019.
[6] L. Sevgi, "Modeling and simulation challenges in wide ocean area surveillance," *IEEE Access*, vol. 7, pp. 117692–117698, 2019.
[7] L. Zhe, Y. Changjun, L. Aijun, Y. Xuguang, and Q. Taifan, "Comparative study on chaos identification of ionospheric clutter from HFSWR," *IEEE Access*, vol. 7, pp. 157437–157448, 2019.
[8] W. Xianrong, C. Feng, and K. Hengyu, "Experimental trials on ionospheric clutter suppression for high-frequency surface wave radar," *IEE Proc.-Radar, Sonar Navigat.*, vol. 153, no. 1, pp. 23–29, Feb. 2006.
[9] R. Riddolls and R. Adve, "Two-dimensional adaptive processing for ionospheric clutter mitigation in high frequency surface wave radar," in *Proc. IEEE Radar Conf.*, Pasadena, CA, USA, May 2009, pp. 127–130.
[10] M. Wu, B. Y. Wen, and H. Zhou, "Ionospheric clutter suppression in HF surface wave radar," *J. Electromagn. Waves Appl.*, vol. 23, no. 10, pp. 1265–1272, Jan. 2009.
[11] T. Wen-Long, L. Gao-Peng, and X. Rong-Qing, "Ionospheric clutter mitigation for high-frequency surface-wave radar using two-dimensional array and beam space processing," *IET Radar Sonar Navigat.*, vol. 6, no. 3, pp. 202–211, 2012.
[12] F. Jangal, S. Saillant, and M. Hélier, "Ionospheric clutter mitigation using one-dimensional or two-dimensional wavelet processing," *IET Radar, Sonar Navigat.*, vol. 3, no. 2, pp. 112–121, 2009.
[13] Y. Su, Y. Wei, R. Xu, and Y. Liu, "Ionospheric clutter suppression using wavelet oblique projecting filter," in *Proc. IEEE Radar Conf. (RadarConf)*, May 2017, pp. 1552–1556.
[14] Y. Abramovich, S. Anderson, Y. Lyudviga, N. Spencer, P. Turcaj, and B. Hibble, "Space-time adaptive techniques for ionospheric clutter mitigation in HF surface wave radar systems," in *Proc. Int. Radar Conf.*, 2004, pp. 1–7.
[15] Z. Xin, Y. Qiang, S. Yanhua, D. Weibo, and D. Yingning, "Space-time adaptive processing-based algorithm for meteor trail suppression in high-frequency surface wave radar," *IET Radar, Sonar Navigat.*, vol. 9, no. 4, pp. 429–436, Apr. 2015.
[16] X. P. Mao, A.-J. Liu, H.-J. Hou, H. Hong, R. Guo, and W.-B. Deng, "Oblique projection polarisation filtering for interference suppression in high-frequency surface wave radar," *IET Radar Sonar Navigat.*, vol. 6, no. 2, pp. 71–80, 2012.
[17] X. Mao, H. Hong, W. Deng, and Y. Liu, "Research on polarization cancellation of nonstationary ionosphere clutter in HF radar system," *Int. J. Antennas Propag.*, vol. 2015, no. 2015, pp. 1–12, 2015.
[18] Y.-M. Wang, X.-P. Mao, H. Hong, J. Zhang, and Y.-M. Cui, "A generalized oblique projection filter with flexible parameter for interference suppression," *Int. J. Antennas Propag.*, vol. 2015, pp. 1–11, May 2015.
[19] H. Mott, *Remote Sensing With Polarimetric Radar*. Hoboken, NJ, USA: Wiley, 2007.
[20] R. T. Behrens and L. L. Scharf, "Signal processing applications of oblique projection operators," *IEEE Trans. Signal Process.*, vol. 42, no. 6, pp. 1413–1424, Jun. 1994.
[21] R. Schmidt, "Multiple emitter location and signal parameter estimation," *IEEE Trans. Antennas Propag.*, vol. 34, no. 3, pp. 276–280, Mar. 1986.
[22] X. Guo, H. Sun, and T. Soon Yeo, "Interference cancellation for high-frequency surface wave radar," *IEEE Trans. Geosci. Remote Sens.*, vol. 46, no. 7, pp. 1879–1891, Jul. 2008.

[23] H. Hong, X.-P. Mao, and C. Hu, "A multi-domain collaborative filter for HFSWR based on oblique projection," in *Proc. IEEE Radar Conf.*, May 2012, pp. 0907–0912.
[24] H. Hong *et al.*, "Joint filtering of space frequencypolarization domain based on vector sensitive array," in *Proc. IEEE Int. Conf. Instrum., Meas., Comput., Commun. Control*, Beijing, China, Oct. 2011, pp. 670–673.
[25] X.-P. Mao, Y.-L. Yang, H. Hong, and W.-B. Deng, "Multi-domain collaborative filter for interference suppressing," *IET Signal Process.*, vol. 10, no. 9, pp. 1157–1168, Dec. 2016.

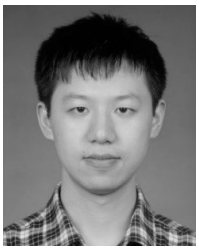

YUNLONG YANG (Student Member, IEEE) was born in Guangxi, China. He received the B.Sc. degree in communication engineering and the M.Sc. degree in electronic and communication engineering from the Harbin Institute of Technology, China, in 2011 and 2014, respectively, where he is currently pursuing the Ph.D. degree in communication and information engineering. His research interests include array design, array signal processing, and signal processing in MIMO networks.

XINGPENG MAO (Member, IEEE) was born in Liaoning, China, in 1972. He received the B.S. degree in radio electronics from Northeast Normal University, Changchun, China, in 1993, and the M.Eng. and Ph.D. degrees in electrical engineering from the Harbin Institute of Technology, Harbin, China, in 1999 and 2004, respectively. He joined the Harbin Institute of Technology as a Lecturer, in 1993, working on the design and development of radar and other electronical system. From 2005 to 2006, he was a Postdoctoral Fellow with the University of Waterloo, Waterloo, ON, Canada. He is currently a Professor with the Department of Electronic and Information Engineering, Harbin Institute of Technology. His current research interests include signal processing in wireless communication and radar. He is a Senior Member of the Chinese Institute of Electronics.

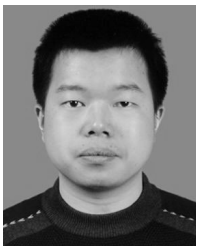

YUGUAN HOU (Member, IEEE) was born in 1979. He received the M.S. and Ph.D. degrees in communication and information system from the Harbin Institute of Technology, China, in 2003 and 2008, respectively. His research interests include array signal processing and statistical signal processing.

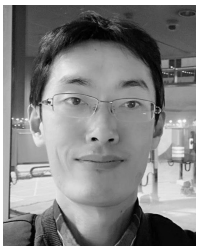

JUN GENG (Member, IEEE) received the B.E. and M.E. degrees from the Harbin Institute of Technology, Harbin, China, in 2007 and 2009, respectively, and the Ph.D. degree from the Worcester Polytechnic Institute, Worcester, MA, USA, in 2015. Since June 2015, he has been an Associate Professor with the Harbin Institute of Technology. His research interests include stochastic signal processing and wireless communications and other related areas.